The Astrophysical Journal Letters, 728:L21 (5pp), 2011 February 10 doi:10.1088/2041-8205/728/1/L21


# PLASMA NEAR THE HELIOSHEATH: OBSERVATIONS AND MODELING

Sergey N. Borovikov[1], Nikolai V. Pogorelov[1,4], Leonard F. Burlaga[2], and John D. Richardson[3]
[1] The University of Alabama in Huntsville, CSPAR, Huntsville, AL 35805, USA
[2] Geospace Physics Laboratory, Code 673, NASA Goddard Space Flight Center, Greenbelt, MD 20771, USA
[3] Kavli Center for Astrophysics and Space Science, Massachusetts Institute of Technology, Cambridge, MA 02139, USA
*Received 2010 October 27; accepted 2010 December 13; published 2011 January 24*

## ABSTRACT

Sound numerical modeling is capable of providing important predictive information about the solar wind interaction with the local interstellar medium. The results of our three-dimensional simulation show a good agreement with *Voyager* observations from 2007 to 2010. We analyze the termination shock properties at the *Voyager* crossing points and juxtapose them with the observed data. The heliospheric current sheet structure in the inner heliosheath is examined.

*Key words:* interplanetary medium – magnetic fields – solar wind – Sun: heliosphere

*Online-only material:* color figures

## 1. INTRODUCTION

The outer heliosphere is the region of space around the Sun which is affected by the interaction of the solar wind (SW) with the local interstellar medium (LISM). The collision of a supersonic SW flow and the supersonic LISM flow results in a tangential discontinuity, the heliopause (HP), which separates these flows, a heliospheric termination shock (TS), and possibly a bow shock (BS). The region between the TS and the HP is called the inner heliosheath (IHS). In 2004 December, *Voyager 1* (*V1*) crossed the TS and became the first man-made object ever to enter the IHS. Unfortunately, only limited data are available for analysis from the *V1* measurements because its plasma instrument has not been operational since 1981. Three years later, on 2007 August 31, *Voyager 2* (*V2*) also crossed the TS, providing the first in situ plasma observations of the TS and IHS. The *Voyager* magnetic field measurements were analyzed in detail by Burlaga et al. (2005, 2008). The *V2* measurements of the IHS parameters show that plasma flow downstream of the TS remains supersonic (Richardson et al. 2008) if the Mach number were calculated using SW protons. Only 20% of the SW kinetic energy is transferred by the TS into internal energy. Energetic particles above 28 keV gained an additional 10% of the kinetic energy. Richardson et al. (2008) suggested that, as predicted by Zank et al. (1996a), the missing energy is accumulated in energetic (4–20 keV) ions (pick-up ions, PUIs), whose properties are not measured by *V2*. Another interesting and puzzling observation from the *V2* plasma experiment revealed an essentially constant plasma speed for a year after the TS crossing and quasi-periodic oscillations of the latitudinal component of the velocity with a period about 115 days (Richardson et al. 2009; Richardson & Wang 2010). Solar cycle effects (Pogorelov et al. 2009b) may be responsible for the former observation, while the latter may be consequences of the HP instability (Borovikov et al. 2008).

In this Letter, we analyze plasma and magnetic field distributions in the heliosheath using a fully three-dimensional numerical model based on a multifluid description of the interacting SW and LISM ions that incorporates both the interplanetary and interstellar magnetic fields (ISMF; Pogorelov et al. 2006, 2007, 2009a). The source terms due to charge exchange between hydrogen ions and neutral H are taken from Pauls et al. (1995) and Zank et al. (1996b). The inner boundary condition in this calculation is at $R_{\rm in} = 12$ AU from the Sun. The 1 AU SW is propagated to 12 AU assuming adiabatic flow. The SW is assumed to be spherically symmetric with the parameters obtained by averaging *IMP 8* data over several solar cycles (Izmodenov et al. 2004): number density $n_{\rm E} = 7.4\,{\rm cm}^{-3}$, radial velocity $u_{\rm E} = 450\,{\rm km\,s}^{-1}$, and temperature $T_{\rm E} = 5.1\times10^5$ K. The radial component of the interplanetary magnetic field (IMF) at 1 AU is 37.5 $\mu$G. The IMF at $R = R_{\rm in}$ is taken to be in the form of a Parker spiral (Parker 1961). The tilt angle between rotation and dipole axes is 30°. We choose the following parameters of the unperturbed LISM: proton number density $n_\infty = 0.06\,{\rm cm}^{-3}$, neutral H density $n_{\rm H\infty} = 0.15\,{\rm cm}^{-3}$, velocity $u_\infty = 26.4\,{\rm km\,s}^{-1}$, proton temperature $T_\infty = 6527$ K, and magnetic field strength $B_\infty = 3\,\mu$G. The LISM vector $\mathbf{V}_\infty$ is aligned with the neutral He velocity vector, $\mathbf{V}_{\rm He}$, calculated from the ultraviolet backscattered observations made by the *Solar and Heliospheric Observatory* (*SOHO*) and the *Extreme-Ultraviolet Explorer* (*EUVE*) satellites (Möbius et al. 2004). The arrival direction of the interstellar neutral helium was found to be $(\lambda, \beta)_{\rm He} = (255.^\circ4, 5.^\circ2)$ in the Heliocentric Aries Ecliptic ($\rm HAE_{J2000}$) coordinates resulting in $\mathbf{l}_{\rm He} = (0.996, -0.018, -0.089)$ in the Heliographic Inertial frame ($\rm HGI_{J2000}$). The velocity $\mathbf{V}_{\rm He}$ of the unperturbed LISM and the direction that neutral hydrogen enters the IHS (the angle between these directions about 5°) determine a so-called hydrogen deflection plane (HDP; Lallement et al. 2005, 2010). We assume that the ISMF vector $\mathbf{B}_\infty$ is in the HDP and directed toward the southern hemisphere at an angle 30° to $\mathbf{V}_{\rm He}$. In $\rm HGI_{J2000}$ coordinates, the normalized ISMF vector has the following direction: $\mathbf{l}_{B_\infty} = (0.825, -0.368, -0.429)$. In our simulations, we use a Sun-centered coordinate system, where the *Z*-axis is the Sun's rotation axis, the *XY*-plane coincides with the solar equatorial plane, and the *XZ*-plane contains $\mathbf{V}_{\rm He}$ vector.

## 2. TERMINATION SHOCK

The TS is a discontinuity created when the supersonic SW encounters the HP. Here the magnetized SW flow slows down, deflects, and experiences compression, heating, and an increase

[4] Also at Physics Department, The University of Alabama in Huntsville, Huntsville, AL 35805, USA.

**Table 1**
Termination Shock Properties at *Voyager 1* and *Voyager 2* Crossing Points

| Parameter | *V1* Simulation | *V2* Simulation | *V2* Measurements |
|---|---|---|---|
| $\mathbf{B}_1$ (nT) | (−0.0005, 0.041, 0.0) | (0.00049, −0.043, 0) | (−0.006, −0.029, 0.012) ±0.03 |
| $\mathbf{B}_2$ (nT) | (−0.007, 0.133, 0.001) | (−0.0093, −0.142, 0.0012) | (0.001, −0.073, −0.018) ±0.03 |
| $\lvert\mathbf{B}_1\rvert$, $\lvert\mathbf{B}_2\rvert$ (nT) | 0.04, 0.13 | 0.04, 0.14 | 0.047, 0.136 ± 0.04 |
| $n_1$, $n_2$ (cm$^{-3}$) | 0.0012, 0.0038 | 0.0012, 0.0039 | 0.0011, 0.0021 |
| $\mathbf{V}_1$ (km s$^{-1}$) | (377, 0.09, 2.9) | (382, 2.4, −3) | (386, 3, −11) |
| $\mathbf{V}_2$ (km s$^{-1}$) | (124,−20, 42) | (122, 32, −29) | (135, 44, −22) |
| $\lvert\mathbf{V}_1\rvert$, $\lvert\mathbf{V}_2\rvert$ (km s$^{-1}$) | 377, 132 | 382, 130 | 387, 144 |
| **n** | (0.9859, 0.0741, −0.1502) | (0.9905, −0.0955, 0.0986) | (0.991, 0.131, 0.013) |
| $\theta_1$, $\theta_2$ | 85.8, 82.1 | 84.5, 88.3 | 82.8, n/a |
| $M_{f1}$, $M_{f2}$ | 3.73, 0.58 | 3.92, 0.56 | 4.9, 1.1 |
| $R_T$, $R_N$ (AU) | 120, 122 | 108, 112 | n/a |
| TS, HP dist. (AU) | 87, 142 | 85, 135 | 84, n/a |

**Notes.** Columns 2 and 3 show the TS parameters obtained from the simulation, and Column 4 contains the TS properties observed by *Voyager 2*, where $n$ is the number density, **n** is the shock normal vector, $\theta$ is the angle between shock normal and magnetic field, $M_f$ is the fast Mach number, and $R$ are the radii of curvature of the TS in the $T$ and $N$ directions. The last line indicates the distances to the TS and HP in the directions of the spacecraft trajectories. All vectors are given in *RTN* coordinates. Indices "1" and "2" refer to parameters ahead of and behind the shock.

in the IMF strength. Our three-dimensional model of the heliosphere makes it possible to compare the TS parameters with the *Voyager* observations summarized in Table 1, where Columns 2 and 3 show the preshock (subscript 1) and postshock (subscript 2) quantities in our simulation at the *V1* and *V2* crossing points, respectively. Column 4 shows the values detected by *V2*. All vectors are given in the *RTN* coordinate system, where the *R*-axis is directed radially away from the Sun, the *T*-axis is the cross product of the solar rotation axis and the *R*-axis, and the *N*-axis completes the right coordinate system.

The magnetic field magnitude, density, and velocity quantities in Column 4 were obtained by averaging *V2* observations between 2007 January 1 and 2007 June 10 for the preshock values and between 2007 September 15 and 2007 December 31 for the postshock parameters. The time interval between 2007 June 11 and 2007 September 14 was skipped to avoid the highly transient shock structure, which is not captured by MHD models. The magnetic field components were averaged separately for $B_T > 0$ and $B_T < 0$ in the intervals above giving the results in Table 1.

The first three rows in Table 1 refer to the IMF vector. The *T*-component, which is dominant in the expanding SW, reasonably well agrees with the observations before and after the TS. The $1\sigma$ uncertainty of measuring the *R*- and *N*-components is ±0.03 nT in the *V2* measurements. It is therefore not surprising that the agreement between the calculated and measured values is not as good as for the *T*-component. The computed ratios of the magnetic field magnitude $B_2/B_1$ in the model are 3.25 and 3.5 in the *V1* and *V2* directions, respectively. These ratios agree well with the *V1* (Burlaga et al. 2005) and *V2* observations (Table 1).

The number density $n_1$ ahead the shock is correctly modeled by the simulation, whereas the number density $n_2$ behind the shock is about 46% of that predicted. The discrepancy may be attributed to inward shock motion. The calculated velocities are also consistent with the observations. The fast Mach number $M_{f1}$ ahead of the shock also agrees with the *V2* measurements (Li et al. 2008). However, the fast Mach number $M_{f2}$ behind the shock is higher than predicted by the simulations. This discrepancy is primarily due to the presence of PUIs, whose temperature is not measured by the spacecraft (Richardson et al. 2008). In our model, we take into account PUIs energetically by solving the system for the mixture of genuine SW protons and PUIs. The effect of the TS motion is less important than the PUIs effects.

The vector **n**, which is the shock normal, was calculated using the velocity-magnetic field coplanarity conditions as in Abraham-Shrauner (1972):

$$\hat{n} = \frac{\mathbf{B_1} \times (\mathbf{V}_2 - \mathbf{V}_1) \times (\mathbf{B}_2 - \mathbf{B}_1)}{|\mathbf{B_1} \times (\mathbf{V}_2 - \mathbf{V}_1) \times (\mathbf{B}_2 - \mathbf{B}_1)|}.$$

This method is more robust to numerical errors than the magnetic coplanarity theorem (Colburn & Sonett 1966) since we do not have to compute the $\mathbf{B}_1 \times \mathbf{B}_2$ vector, which is close to zero for quasi-perpendicular shocks. The normal can be also estimated using a geometrical reconstruction of the shock from the simulation. To determine which approximation to the normal is better, we calculated the discrepancy in the satisfaction of the Rankine–Hugoniot relations and found that the discrepancy is about 10 times larger for the case of geometrical reconstruction than for the Abraham-Shrauner formula. The reason is that our numerical scheme ensures the accurate satisfaction of the conservation laws across the shock. On the contrary, the points, belonging to the TS cannot be identified as accurately as plasma quantities due to numerical dissipation in the near vicinity of the shock. It is well known from computational geometry that geometrical algorithms are extremely sensitive to round-off errors. Therefore, uncertainties in the TS position introduce a larger error in the normal determination.

The calculated shock normal is only slightly different from the observed normal (Li et al. 2008). The angle $\theta_1$ between the shock normal **n** and magnetic field ahead the TS is also very close to that detected by *V2* (Richardson et al. 2008). However, uncertainties in the measured components of the IMF do not allow us to derive **n** and $\theta_1$ reliably from the observations. The similar angle $\theta_2$ between the magnetic field behind the shock and its normal was not measured.

The $R_T$ and $R_N$ parameters in Table 1 show the radii of curvature of the TS in the *N* and *T* directions, respectively. The *RN* coordinate plane intersects the TS along a curve, whose radius of curvature $R_N$ can be easily estimated at the *V1* and *V2* TS crossings. The intersection between the TS and a plane that is perpendicular to the *RN* plane and passes through the coordinate center results in a curve, whose radius of curvature

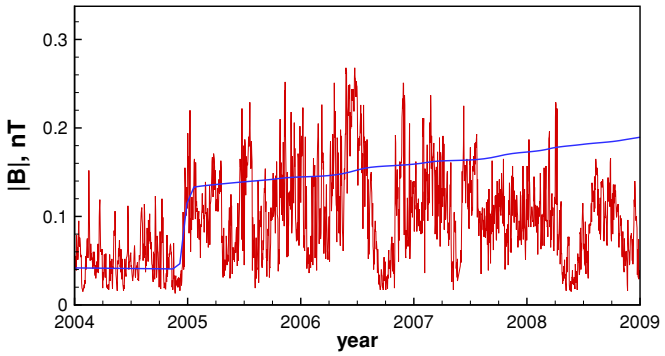


**Figure 1.** *Voyager 1* observations of daily averages of the magnetic field (red line) and magnetic field strength from the simulations.

(A color version of this figure is available in the online journal.)

$R_T$ is also calculated. The radius of curvature is larger than that of a similar size sphere, which is consistent with the TS being blunt. Zank (1999) and Jokipii et al. (2004) suggested that the effect of this bluntness can be important for the interpretation of streaming anisotropies of energetic ions observed by *Voyagers* (Opher et al. 2006; Pogorelov et al. 2007; Müller et al. 2008). However, the calculations do not support a suggestion that the shock is blunter (i.e., radius is larger) in the *T* direction than in the *N* direction (Richardson et al. 2009). The curvature radii are similar in the *T* and *N* directions, but different at the *V1* and *V2* crossing points.

## 3. DISTRIBUTIONS IN THE HELIOSHEATH

The *Voyager 1* has been measuring magnetic fields in the heliosheath since 2004 December. Daily averages of the *V1* magnetic field strength observations are shown in Figure 1. Burlaga et al. (2009) showed that between 2005.0 and 2008.82, when *V1* moved from 94.22 to 107.9 AU, the gradient of the magnetic field strength was $0.0036 \pm 0.0019$ nT AU$^{-1}$, after correcting for the effects of decreasing solar activity. Our model predicts a radial gradient 0.004 nT AU$^{-1}$ in good agreement with the observations made within this period of time.

Figure 2 shows *V2* daily averages of the three velocity components. The *R*- and *N*-components of the velocity show reasonably good agreement with the simulations, whereas the *T*-component is approximately twice as large as predicted by these simulations. Figure 3 shows the flow angles in the heliosheath. As seen from both observations and simulations, the angles increase as *V2* moves deeper into the heliosheath. In our simulations, we use steady SW parameters at the inner boundary and get a steady TS in our solution. However, declining solar activity in 2007–2009 caused a gradual decrease in the SW dynamic pressure (Richardson et al. 2006) and an inward motion of the TS with a speed of about 13.8 km s$^{-1}$. This inward motion was used to correct the deflection angles (Figure 3, dashed line). The updated flow deflection angles match the observations much better, which speaks of the importance of time-dependent phenomena occurring in the IHS.

## 4. HELIOSPHERIC CURRENT SHEET AND SECTOR STRUCTURE IN THE HELIOSHEATH

The angle between the Sun's rotation and magnetic-dipole axis is not zero, varying from about 8°–9° during solar minima to 90° at solar maxima as a result of the Sun's rotation. The heliospheric current sheet (HCS) naturally forms and bears the

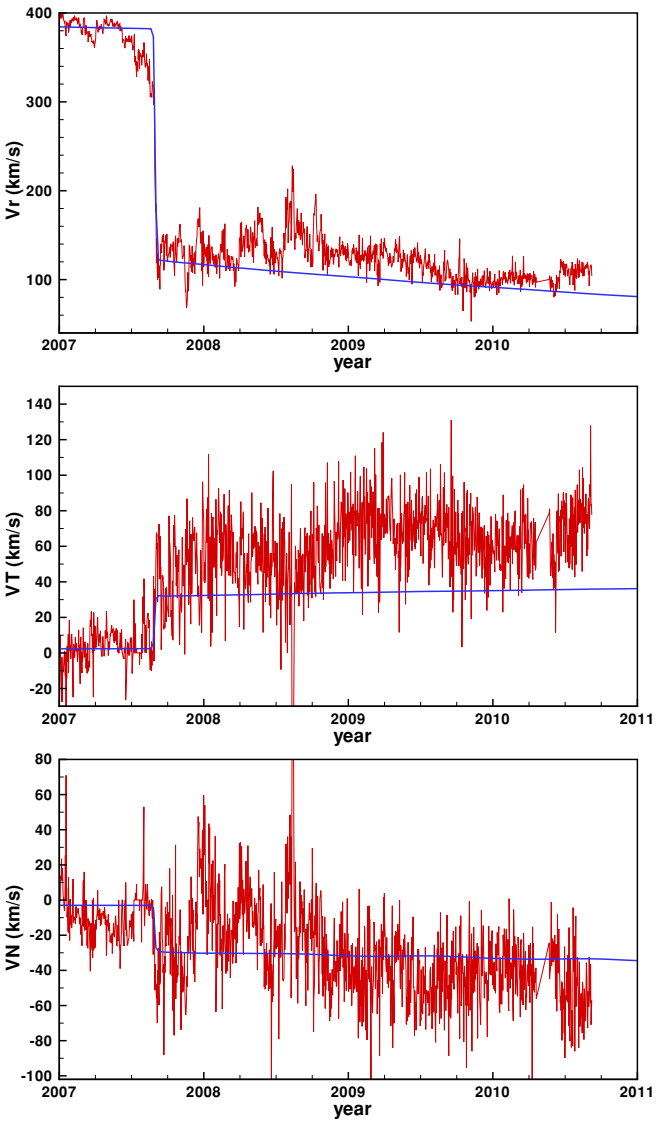


**Figure 2.** *Voyager 2* observations of daily averages of the three velocity components (red line) and the same components obtained from the simulations.

(A color version of this figure is available in the online journal.)

imprint of the Sun's rotation. The HCS separates the regions of opposite IMF polarity, which are observed as unipolar sectors. Modeling the global behavior of the HCS is a computationally challenging problem. If the SW velocity is 450 km s$^{-1}$, the distance between two consecutive crossings of the equatorial plane by the HCS (the size of the sector) is about 3.3 AU. As the SW propagates from the Sun, being decelerated by charge exchange with the interstellar neutrals, the equatorial thickness of each sector decreases to 2.78 AU ahead the TS and 0.84 AU behind it. Farther in to the heliosheath, the thickness of the sectors continues to decrease proportional to the radial velocity and reaches 0.07 AU at 120 AU. Ultimately, the size of the sector becomes close to zero near the HP and can no longer be resolved.

Here, we adopt a kinematic approach assuming that the HCS advects with the local SW velocity. This allows us to apply the level set method (Osher & Fedkiw 2002; Sethian 1999), which is widely used for tracking surfaces. The idea of the method is the following. Suppose the velocity field distribution $\mathbf{V}(x, y, z, t)$ is known and the initial surface position $s_0(x, y, z) = 0$ is given at $t = 0$. In the kinematic approximation, the points belonging to the surface move at a given velocity, and one can find a new

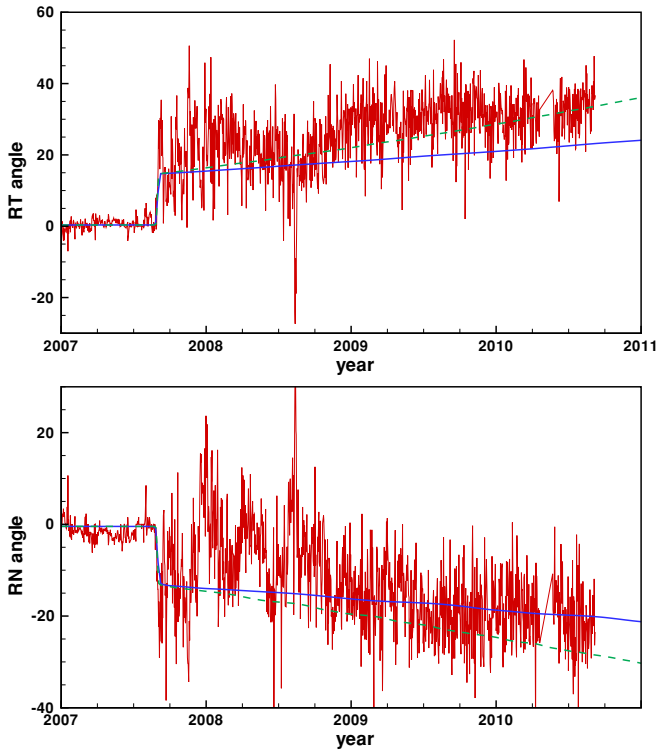


**Figure 3.** *Voyager 2* observations of daily averages of the flow angles (red line) and the same components obtained from the simulations. The green dashed line shows flow angles if the TS moves inward with the speed about 13.8 km $s^{-1}$.

(A color version of this figure is available in the online journal.)

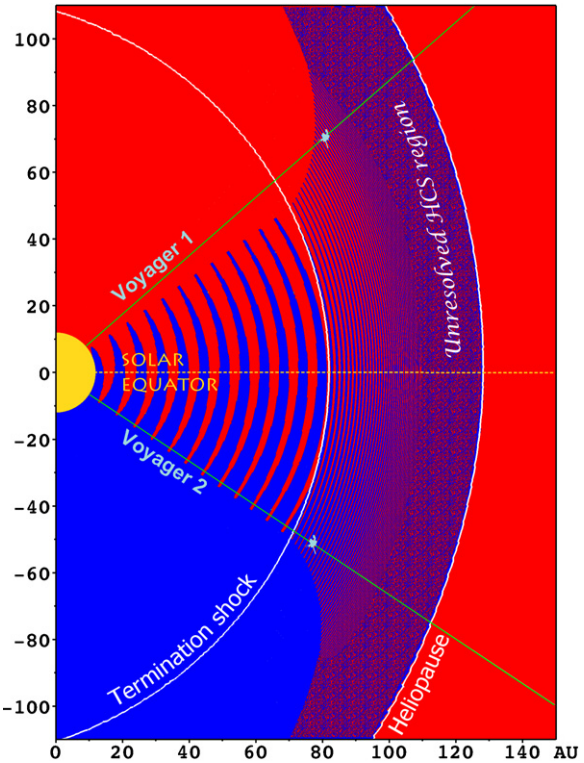


**Figure 4.** HCS structure in the plane formed by the current *V1* and *V2* trajectories. The *Voyager* locations are given on 2010 July 1. The tilt of the Sun's magnetic axis to its rotation axis is 30°.

(A color version of this figure is available in the online journal.)

surface position $s(x, y, z, t) = 0$ at $t > 0$ by solving a simple advection equation:

$$s_t + \mathbf{V} \cdot \nabla s = 0.$$

The IMF in the interplanetary space is frozen in to the SW plasma; therefore, the HCS is passively advected by the SW flow. If we introduce a level set function

$$s(x, y, z, t) = \begin{cases} -1 & \text{if } B_R \leqslant 0 \\ 1 & \text{if } B_R > 0 \end{cases}$$

and solve the advection equation together with the ideal MHD equations, the isosurface $s = 0$ determines the HCS shape in three-dimensional space. This approach allows us to apply state-of-the-art techniques developed for surface tracking (Osher & Fedkiw 2002). As a result, the HCS resolution greatly improves as compared with the standard ideal MHD approach. Another method to determine the HCS shape is based on tracking a neutral line originating from the inner boundary in the Lagrangian reference frame (Czechowski et al. 2010). This method gives better resolution; however, extra efforts are required to calculate the sign of the magnetic field polarity at a given point in space. This makes application of this method more computationally difficult for problems that require magnetic field reversals to be taken into account, compared with the level set method where the polarity is automatically known from the level set function.

Figure 4 shows the HCS structure in the plane formed by the current *V1* and *V2* trajectories. The mentioned approach allows us to resolve HCS structure up to 120 AU both in the *V1* and *V2* directions. This resolution seems to be acceptable because the kinematic approximation can be justified only at some distance from the HP, where the effects of magnetic field on the SW flow are minor. The *Voyagers* positions on 2010 July 1 are shown. Our estimates show that in the IHS *V2* spends 21% of the time in the region with the magnetic field polarity originating from the southern hemisphere. This fact agrees well with the estimates of Burlaga et al. (2010). Our estimates predict that *V1* should have started observing both magnetic field polarities in 2009 day-of-year 150 due to a northward flow in the heliosheath. This prediction was supported by the observations (Burlaga & Ness 2010).

## 5. CONCLUSION

In this Letter, we compared the simulation results from our multifluid model of the SW–LISM interaction with *V1* and *V2* observations at the TS and in the IHS. Being extremely important for the model validation, our analysis showed a good agreement in the SW-averaged quantities observed by *V2*. The gradients of magnetic field strength and velocity are also well reproduced. It is not possible to compare the SW temperatures in the IHS since our model provides the temperature of the proton–PUI mixture, while the *Voyager* spacecraft are measuring thermal SW protons only. A meaningful comparison of point-to-point measurements with calculations is not possible not only because of our boundary conditions being stationary, but also because of the absence of self-consistent three-dimensional boundary conditions.

This work was supported by NASA grants NNX09AG63G, NNX09AW44G, NNX09AP74A. Calculations were performed on supercomputers from NASA(SMD-09-1148), NSF (MCA07S033), and DOE (PSS003). J.D.R. was supported by NASA's *Voyager* project and NASA grant NNX08AC04G.

## REFERENCES


Abraham-Shrauner, B. 1972, J. Geophys. Res., 77, 736
Borovikov, S. N., Pogorelov, N. V., Zank, G. P., & Kryukov, I. A. 2008, ApJ, 682, 1404
Burlaga, L. F., & Ness, N. F. 2010, ApJ, 725, 1306
Burlaga, L. F., Ness, N. F., Acuña, M. H., Lepping, R. P., Connerney, J. E. P., & Richardson, J. D. 2008, Nature, 454, 75
Burlaga, L. F., Ness, N. F., Acuña, M. H., Lepping, R. P., Connerney, J. E. P., Stone, E. C., & McDonald, F. B. 2005, Science, 309, 2027
Burlaga, L. F., Ness, N. F., Acuña, M. H., Wang, Y., & Sheeley, N. R. 2009, J. Geophys. Res. (Space Phys.), 114, 6106
Burlaga, L. F., Ness, N. F., Wang, Y., Sheeley, N. R., & Richardson, J. D. 2010, J. Geophys. Res. (Space Phys.), 115, 8107
Colburn, D. S., & Sonett, C. P. 1966, Space Sci. Rev., 5, 439
Czechowski, A., Strumik, M., Grygorczuk, J., Grzedzielski, S., Ratkiewicz, R., & Scherer, K. 2010, A&A, 516, A17
Izmodenov, V., Malama, Y., Gloeckler, G., & Geiss, J. 2004, A&A, 414, L29
Jokipii, J. R., Giacalone, J., & Kóta, J. 2004, ApJ, 611, L141
Lallement, R., Quémerais, E., Bertaux, J. L., Ferron, S., Koutroumpa, D., & Pellinen, R. 2005, Science, 307, 1447
Lallement, R., Quémerais, E., Koutroumpa, D., Bertaux, J., Ferron, S., Schmidt, W., & Lamy, P. 2010, in AIP Conf. Proc. 1216, Twelfth International Solar Wind Conference, ed. M. Maksimovic et al. (Melville, NY: AIP), 555
Li, H., Wang, C., & Richardson, J. D. 2008, Geophys. Res. Lett., 35, 19107
Möbius, E., et al. 2004, A&A, 426, 897
Müller, H., Florinski, V., Heerikhuisen, J., Izmodenov, V. V., Scherer, K., Alexashov, D., & Fahr, H. 2008, A&A, 491, 43
Opher, M., Stone, E. C., & Liewer, P. C. 2006, ApJ, 640, L71
Osher, S. J., & Fedkiw, R. P. 2002, Level Set Methods and Dynamic Implicit Surfaces (New York: Springer-Verlag)
Parker, E. N. 1961, ApJ, 134, 20
Pauls, H. L., Zank, G. P., & Williams, L. L. 1995, J. Geophys. Res., 100, 21595
Pogorelov, N. V., Borovikov, S. N., Florinski, V., Heerikhuisen, J., Kryukov, I. A., & Zank, G. P. 2009a, in ASP Conf. Ser. 406, Numerical Modeling of Space Plasma Flows, ed. N. V. Pogorelov et al. (San Francisco, CA: ASP), 149
Pogorelov, N. V., Borovikov, S. N., Zank, G. P., & Ogino, T. 2009b, ApJ, 696, 1478
Pogorelov, N. V., Stone, E. C., Florinski, V., & Zank, G. P. 2007, ApJ, 668, 611
Pogorelov, N. V., Zank, G. P., & Ogino, T. 2006, ApJ, 644, 1299
Richardson, J. D., Kasper, J. C., Wang, C., Belcher, J. W., & Lazarus, A. J. 2008, Nature, 454, 63
Richardson, J. D., Stone, E. C., Kasper, J. C., Belcher, J. W., & Decker, R. B. 2009, Geophys. Res. Lett., 36, 10102
Richardson, J. D., & Wang, C. 2010, ApJ, 711, L44
Richardson, J. D., Wang, C., & Zhang, M. 2006, in AIP Conf. Ser. 858, Physics of the Inner Heliosheath, ed. J. Heerikhuisen et al. (Melville, NY: AIP), 110
Sethian, J. A. 1999, Level Set Methods and Fast Marching Methods (Cambridge: Cambridge Univ. Press)
Zank, G. P. 1999, Space Sci. Rev., 89, 413
Zank, G. P., Pauls, H. L., Cairns, I. H., & Webb, G. M. 1996a, J. Geophys. Res., 101, 457
Zank, G. P., Pauls, H. L., Williams, L. L., & Hall, D. T. 1996b, J. Geophys. Res., 101, 21639